Efficient Transient Thermal Simulation of ICs and Packages With Laguerre-Based Finite-Element Method

Bo Li, Min Tang, *Member, IEEE*, Haikun Yue, Yang Tang, and Junfa Mao, *Fellow, IEEE*

***Abstract*— In this article, an efficient approach based on Laguerre-based finite-element method (LBFEM) is proposed for transient thermal simulation of integrated circuits (ICs) and packages. The unconditionally stable marching-on-in-order scheme is developed by the weighted Laguerre polynomials and Galerkin testing procedure. In order to handle complicated ICs and packages, the finite-element method (FEM) is employed for spatial discretization and to obtain the Laguerre coefficients. The treatment of different kinds of boundary conditions is also discussed in detail. The accuracy and efficiency of the proposed method are demonstrated by numerical examples.**

***Index Terms*— Integrated circuit (IC), Laguerre-based finite-element method (LBFEM), marching-on-in-order scheme, package, transient thermal simulation.**

I. Introduction

THE growing packaging density and power consumption of integrated circuits (ICs) have made the thermal management one of the most important concerns for design of high-performance ICs and systems [1]. Since the junction temperature of the device has a direct impact on the overall system reliability, accurate evaluation of temperature profile of ICs, as well as their packages and systems, is a major task facing design engineers of modern electronic systems.

In the past few decades, a considerable number of algorithms have been devoted to both steady-state and transient thermal modeling of IC chips and packages. Among these approaches, the finite-element method (FEM) [2]–[5], finite volume method (FVM) [6], [7], and finite difference method (FDM) [8], [9] are the most popular ones. For example, an FDM-based thermal solver named "HotSpot" [9], which utilizes the equivalent circuit of thermal resistance and capacitances of microarchitecture blocks, is applied to analyze thermal distributions of ICs. Compared with the FDM-based solvers, both FVM and FEM are more flexible to address complex irregular geometries and thus are widely employed by commercial solvers, such as ANSYS and COMSOL.

For the above-mentioned approaches, large and sparse system stiffness matrices will be constructed based on the low-order finite-difference approximations or localized basis functions. These matrix equations are then solved by iterative algorithms. In transient thermal simulation, implicit schemes such as the backward Euler method and the Crank–Nicolson (CN) method [10] are adopted. Nevertheless, when the objects consist of a large number of unknowns, such as complicated ICs and integrated packages, these conventional methods become time-consuming.

To alleviate this problem, some effective approaches have been developed. For instance, the nonconformal domain decomposition method (DDM) [11]–[13] and Krylov space-based model-order reduction (MOR) technique [14] were proposed to handle system-level thermal modeling of 3-D integrated packages. In [15], the discontinuous Galerkin time-domain (DGTD) algorithm, which can be treated as a kind of element-level DDM, was employed to deal with multiscale geometries in 3-D integrated systems. Nevertheless, due to the explicit scheme in time domain, the time step size should be limited by the well-known Courant–Friedrich–Levy (CFL) stability condition.

As an efficient and unconditionally stable approach, the alternating direction implicit (ADI) scheme has been proposed in [16]. In each time step of transient simulation, the ADI method alternately solves three equations with tridiagonal stiffness matrices. The computational cost is reduced significantly by this scheme. Although it is unconditionally stable, the numerical dispersion error becomes bigger as the time step increases. Recently, another unconditionally stable method with weighted Laguerre polynomials for thermal simulation was introduced in [17]. By using the entire domain Laguerre polynomials for the expansion of the temporal variation, the resulting marching-on-in-order scheme eliminates the time variable and is free of stability issue. The computational efficiency can be improved significantly by this means. Nevertheless, this marching-on-in-order scheme has only been verified in the case where it was combined with the conventional FDM. Since the structures of real integrated packages and systems are rather complicated, it is thus essential to extend the marching-on-in-order scheme with more flexible

Manuscript received November 2, 2019; accepted December 24, 2019. Date of publication December 31, 2019; date of current version February 6, 2020. This work was supported in part by the Science Challenge under Project TZ2018003 and in part by the National Natural Science Foundation of China under Grant 61674105, Grant 61831016, and Grant 61831006. Recommended for publication by Associate Editor L. Choobineh upon evaluation of reviewers' comments. *(Corresponding author: Min Tang.)*

Bo Li, Min Tang, and Junfa Mao are with the Key Laboratory of Ministry of Education of China for Research of Design and Electromagnetic Compatibility of High Speed Electronic Systems, Shanghai Jiao Tong University, Shanghai 200240, China (e-mail: tm222@sjtu.edu.cn).

Haikun Yue and Yang Tang are with the Microsystem and Terahertz Research Center, China Academy of Engineering Physics, Chengdu 611731, China.

Color versions of one or more of the figures in this article are available online at http://ieeexplore.ieee.org.

Digital Object Identifier 10.1109/TCPMT.2019.2963265

platform (e.g., FEM), which is the main motivation of this article.

Besides the hexahedron elements, the FEM uses unstructured grids to model complex geometries and provides a natural way for handling field and flux continuity conditions at material interfaces. Therefore, it is chosen in this article to combine with weighted Laguerre polynomials to derive an unconditionally stable marching-on-in-order scheme for efficient thermal simulation of complicated ICs and packages.

The rest of this article is organized as follows. In Section II, the development of Laguerre-based FEM (LBFEM) is presented. The marching-on-in-order scheme is derived by the weighted Laguerre polynomials and Galerkin testing procedure. The treatment of boundary conditions, as well as the special thin layers, is given in Section III. Numerical examples are provided to validate the accuracy and efficiency of the proposed method in Section IV. Some conclusions are drawn in Section V.

II. Development of LBFEM

The transient heat conduction in an integrated system is governed by the following equation:

$$\rho c\frac{\partial T(\boldsymbol{r},t)}{\partial t}-\nabla\cdot[\kappa(\boldsymbol{r})\nabla T(\boldsymbol{r},t)]=g(\boldsymbol{r},t) \tag{1}$$

where ρ is the density of the material, c is the specific heat, κ is the thermal conductivity, and g is the heat energy generation rate.

Apparently, the heat conduction (1) is a typical partial differential equation. With the conventional numerical methods, it would be discretized in both the spatial and temporal domains, and then solved by a kind of matching-on-in-time scheme to obtain the transient results. However, the stability and numerical dispersion error of the scheme are always troublesome issues.

A. Temporal Basis Functions Expansion Using Weighted Laguerre Polynomials

In order to obtain an unconditionally stable solution regardless of the time step size, the weighted Laguerre polynomials as an entire domain temporal basis function is utilized. Thus, the temperature variable in (1) can be represented by a sum of infinite Laguerre basis function scaled by the corresponding coefficients $T_p\ (r)$ as [17]

$$T(\boldsymbol{r},t)=\sum_{p=0}^{\infty}T_p(\boldsymbol{r})\varphi_p(\bar{t}) \tag{2}$$

where $\bar{t}=t\cdot s$, t is the time and s is the time scaling factor, and subscript p denotes the order of basis function $\varphi_p(\bar{t})$ with the expression

$$\varphi_p(\bar{t})=e^{-\frac{\bar{t}}{2}}L_p(\bar{t}) \tag{3}$$

where the Laguerre polynomials are defined by

$$L_p(t)=\frac{e^t}{p!}\frac{d^p}{dt^p}(e^{-t}t^p)\quad\text{for }(p\geq 0;t>0). \tag{4}$$

The Laguerre polynomials are orthogonal to the weighting function e^{-t} as follows:

$$\int_0^{\infty}e^{-t}L_p(t)L_q(t)dt=\begin{cases}1, & p=q\\ 0, & p\neq q.\end{cases} \tag{5}$$

Based on (2), the first derivative of $T(\boldsymbol{r},\ t)$ with respect to time t is given by

$$\frac{\partial T(\boldsymbol{r},t)}{\partial t}=s\sum_{p=0}^{\infty}\left[0.5T_p(\boldsymbol{r})+\sum_{k=0}^{p-1}T_k(\boldsymbol{r})\right]\varphi_p(\bar{t}). \tag{6}$$

By substituting (2) and (6) into (1), we obtain

$$\rho cs\sum_{p=0}^{\infty}\left(0.5T_p(\boldsymbol{r})+\sum_{k=0}^{p-1}T_k(\boldsymbol{r})\right)\varphi_p(\bar{t})-\nabla\cdot\left[\kappa(\boldsymbol{r})\nabla\left(\sum_{p=0}^{\infty}T_p(\boldsymbol{r})\varphi_p(\bar{t})\right)\right]=g(\boldsymbol{r},t). \tag{7}$$

Then, taking advantage of the orthogonal property of the weighted Laguerre functions, a temporal Galerkin's testing procedure can be utilized to eliminate the time-dependent terms. After multiplying both sides of (7) by $\varphi_q(\bar{t})$ and integrating over the time domain, the resulting equation is given by

$$\rho cs\left[0.5T_q(\boldsymbol{r})+\sum_{k=0}^{q-1}T_k(\boldsymbol{r})\right]-\nabla\cdot[\kappa(\boldsymbol{r})\nabla T_q(\boldsymbol{r})]=g_q(\boldsymbol{r}) \tag{8}$$

where

$$g_q(\boldsymbol{r})=\int_0^{\infty}g(\boldsymbol{r},t)\varphi_q(\bar{t})d\bar{t}.$$

The upper limit of infinity can be replaced by a finite time interval T_f when the heat source has practically decayed to the value of zero.

For clarity, (8) can be rewritten in a recursive form as

$$\alpha T_q(\boldsymbol{r})-\nabla\cdot[\kappa(\boldsymbol{r})\nabla T_q(\boldsymbol{r})]=f_q(\boldsymbol{r}) \tag{9}$$

where

$$\alpha=0.5\rho cs$$
$$f_q(\boldsymbol{r})=g_q(\boldsymbol{r})-\rho cs\sum_{k=0}^{q-1}T_k(\boldsymbol{r}).$$

It is observed that there is no temporal variable in (9) any more. Instead, we only need to solve a set of Laguerre coefficients $T_q\ (\boldsymbol{r})$ recursively when the order of Laguerre basis function q is chosen. The optimum selection of the order is discussed in [18]. Therefore, this approach is not constrained by the size of time step and is free of stability issue.

B. Solving Laguerre Coefficients With FEM

In the following procedure, as a convenient and flexible approach to handle irregular geometries, the FEM is employed to solve (9) for the Laguerre coefficients $T_q\ (\boldsymbol{r})$.

The FEM is a widely used numerical technique for obtaining approximate solutions to boundary-value problems. With

FEM, the whole solution domain is first discretized into many small elements, such as the tetrahedral ones. Then, by introducing the shape function N^e, $T_q\ (\boldsymbol{r})$ of an element can be approximated by a function of its nodal value

$$T_q(\boldsymbol{r}) = \sum_{i=1}^{n} N_i^e T_{q,i} \tag{10}$$

where n is the number of nodes in an element and $T_{q,i}$ is the value at the node.

After that, the Ritz variational or Galerkin's methods can be used to formulate the system of equations. In this article, the Galerkin's method is adopted for this purpose.

The residual associated with (8) is given by

$$R = \alpha T_q(\boldsymbol{r}) - \nabla \cdot [\kappa(\boldsymbol{r}) \nabla T_q(\boldsymbol{r})] - f_q(\boldsymbol{r}). \tag{11}$$

Combining with (10), the weighted residual for element e is

$$\begin{aligned} R_i^e &= \iiint_{V^e} \left(N_i^e \cdot R\right) dV \\ &= \sum_{j=1}^{n} T_{q,j} \iiint_{V^e} \left(\alpha N_i^e N_j^e + \kappa_x \frac{\partial N_i^e}{\partial x} \frac{\partial N_j^e}{\partial x} + \kappa_y \frac{\partial N_i^e}{\partial y} \frac{\partial N_j^e}{\partial y} \right. \\ &\qquad \left. + \kappa_z \frac{\partial N_i^e}{\partial z} \frac{\partial N_j^e}{\partial z} \right) dV \\ &\quad - \iint_{\Omega^e} \left(N_i^e \boldsymbol{D} \cdot \boldsymbol{n}^e\right) dS - \iiint_{V^e} \left(N_i^e f_q\right) dV \end{aligned} \tag{12}$$

where κ_x, κ_y, and κ_z are the thermal conductivities in x-, y-, and z-directions, respectively, $\boldsymbol{\Omega}^e$ is the surface enclosing the volume V^e of element e, $\boldsymbol{n}^e$ is the outward unit vector normal to $\boldsymbol{\Omega}^e$, and

$$\boldsymbol{D} = \left(\kappa_x \frac{\partial N_j^e}{\partial x} \boldsymbol{x} + \kappa_y \frac{\partial N_j^e}{\partial y} \boldsymbol{y} + \kappa_z \frac{\partial N_j^e}{\partial z} \boldsymbol{z} \right). \tag{13}$$

The above equation can be written in a matrix form as

$$\boldsymbol{R}^e = \boldsymbol{K}^e \boldsymbol{T}_q^e - \boldsymbol{b}_q^e - \boldsymbol{f}_q^e \tag{14}$$

where

$$\begin{aligned} \boldsymbol{K}_{i,j}^e &= \iiint_{V^e} \left(\alpha N_i^e N_j^e + \kappa_x \frac{\partial N_i^e}{\partial x} \frac{\partial N_j^e}{\partial x} + \kappa_y \frac{\partial N_i^e}{\partial y} \frac{\partial N_j^e}{\partial y} \right. \\ &\qquad \left. + \kappa_z \frac{\partial N_i^e}{\partial z} \frac{\partial N_j^e}{\partial z} \right) dV \\ \boldsymbol{b}_{q,i}^e &= \iint_{\Omega^e} \left(N_i^e \boldsymbol{D} \cdot \boldsymbol{n}^e\right) dS \\ \boldsymbol{f}_{q,i}^e &= \iiint_{V^e} \left(N_i^e f_q\right) dV. \end{aligned}$$

The resulting equation is then obtained by assembling all the elements, as given by

$$\sum_{e=1}^{M} \left(\boldsymbol{K}^e \boldsymbol{T}_q^e - \boldsymbol{b}_q^e - \boldsymbol{f}_q^e \right) = 0. \tag{15}$$

Thus, the final stiffness matrix equation can be written as

$$\boldsymbol{K}\boldsymbol{T}_q = \boldsymbol{b}_q + \boldsymbol{f}_q. \tag{16}$$

By solving (16) with appropriate boundary conditions, we can get the value of T_q, and the transient evolution process of temperature distribution of the object is readily obtained by (2).

III. Boundary Conditions

The typical boundary conditions for thermal simulation with the proposed LBFEM are discussed as follows.

A. Temperature Boundary

The temperature boundary is also named as Dirichlet boundary with the relation

$$T^{\text{first}} = T|_{\Gamma_1} \tag{17}$$

where $T|_{\Gamma_1}$ is the setting temperature on the boundary Γ_1. Using the Laguerre basis functions, (17) can be converted into the form of Laguerre domain as

$$T_q^{\text{first}} = \int_0^{t_f} T|_{\Gamma_1} \varphi_q(\bar{t}) d\bar{t}. \tag{18}$$

B. Heat-Flux Boundary

The Neumann boundary condition specifies the value of heat flux on the boundary

$$\kappa \left(\frac{\partial T^{\text{second}}}{\partial n}|_{\Gamma_2} \right) = q(t)|_{\Gamma_2} \tag{19}$$

where $q(t)|_{\Gamma_2}$ is the heat flux on the boundary surface Γ_2.

By applying the Laguerre basis functions in (19) and introducing the shape function N^s on the surface elements, the resulting modified terms of $\boldsymbol{b}_q$ in (16) can be calculated by

$$b_{q,i}^s|_{\Gamma_2} = \iint q_q|_{\Gamma_2} N_i^s dS, \quad i = 1, 2, \ldots, n_s \tag{20}$$

where

$$q_q|_{\Gamma_2} = \int_0^{t_f} q(t)|_{\Gamma_2} \varphi_q(\bar{t}) d\bar{t}$$

and n_s is the number of nodes in a boundary element.

C. Convection Boundary

The convection boundary is a kind of nonhomogeneous Neumann boundary condition, which describes the heat exchange between the boundary surface and environment. It is given by

$$\kappa \left(\frac{\partial T^{\text{third}}}{\partial n}|_{\Gamma_3} \right) = -h(T^{\text{third}} - T^{\text{amb}}|_{\Gamma_3}) \tag{21}$$

where $T^{\text{amb}}|_{\Gamma_3}$ is the ambient temperature and h is the convection heat transfer coefficient.

With the Laguerre basis functions and the shape functions on the surface elements, the impact of convection boundary (21) can be transformed into the modification of corresponding terms of $\boldsymbol{K}$ and $\boldsymbol{b}_q$ in (16) as

$$K_{ij}^s|_{\Gamma_3} = \iint h N_i^s N_j^s dSi, \quad j = 1, 2, \ldots, n_s \tag{22}$$

$$b_{q,i}^s|_{\Gamma_3} = \iint h T_q^{\text{amb}}|_{\Gamma_3} N_i^s dS, \quad i = 1, 2, \ldots, n_s \tag{23}$$

where

$$T_q^{\text{amb}}|_{\Gamma_3} = \int_0^{t_f} T^{\text{amb}}|_{\Gamma_3}\varphi_q(\bar{t})d\bar{t}.$$

D. Thin-Layer Boundary Condition

In practical cases, some special thin layers that conduct heat well need not be defined in 3-D models. Alternatively, they are more suitable to be treated as the thin-layer boundary conditions in thermal simulations.

The governing equation of thin layer boundary Γ_{tl} is described by

$$\kappa\left(\frac{\partial T^{tl}}{\partial n}|_{\Gamma_{tl}}\right) = -\rho_s c_s d_s\left(\frac{\partial T^{tl}(t)}{\partial t}\right) + \nabla\cdot[d_s\kappa_s\nabla T^{tl}(t)] \quad (24)$$

where ρ_s is the density, c_s is the specific heat, κ_s is the thermal conductivity, and d_s is the thickness of thin layer.

With the Laguerre basis functions, (24) can be transformed into the following equation:

$$\kappa\left(\frac{\partial T_q^{tl}}{\partial n}|_{\Gamma_{tl}}\right) = -\alpha_s T_q^{tl} - f_{q,s} + \nabla\cdot\left[d_s\kappa_s\nabla T_q^{tl}\right] \quad (25)$$

where

$$\alpha_s = 0.5\rho_s c_s d_s s$$
$$f_{q,s} = \rho_s c_s d_s s\sum_{k=0}^{q-1} T_k^{tl}.$$

Then, by introducing the shape functions in (25) and following the procedure of FEM, the resulting modification of the terms of $\boldsymbol{K}$ and $\boldsymbol{b}_q$ in (16) can be written as

$$K_{ij}^s|_{\Gamma_{tl}} = \iint d_s\kappa_s\left(\frac{\partial N_i^s}{\partial x}\frac{\partial N_j^s}{\partial x} + \frac{\partial N_i^s}{\partial y}\frac{\partial N_j^s}{\partial y}\right)dS + \iint \alpha_s N_i^s N_j^s dS, \quad i,j = 1,2,3 \quad (26)$$

and

$$b_{q,i}^s|_{\Gamma_{tl}} = \iint f_{q,s}N_i^s dS, \quad i = 1,2,3. \quad (27)$$

IV. Numerical Results

In this section, several examples on the transient thermal issues of ICs and packages are provided to verify the accuracy and efficiency of the proposed algorithm. All the examples are performed on a server with two Intel Xeon E5-2695 CPUs (2.10 GHz), and 256-GB memory.

A. FOWLP on Circuit Board

In the first case, a fan-out wafer-level packaging (FOWLP) is analyzed. Fig. 1 represents a printed circuit board (PCB) with a FOWLP mounted by means of solder ball joints. The dimensions of the chip in the package are $5 \times 5 \times 0.15$ mm^3. The molded package size is 7×7 mm^2, with a thickness of 0.35 mm. The package/chip area ratio is 1.96. The package is with 10×10 solder balls (0.3-mm diameter and 0.7-mm pitch), which are reflowed on the circuit board. The dimensions of PCB are $10 \times 10 \times 0.8$ mm^3. Note that due to the thin conducting layer, the top plane (with a thickness of 0.05 mm) of PCB is modeled using a 2-D shell approximation with the thin-layer boundary condition. For thermal simulation, the materials and corresponding thermal properties for all components of this structure are listed in Table I.

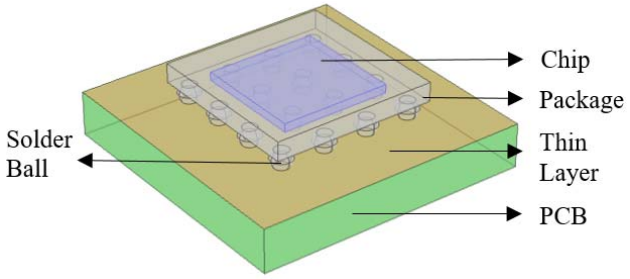

Fig. 1. Schematic of the surface mount package.

TABLE I
Thermal Properties of Materials

Component	Material	Thermal Conductivity (W/m · K)	Thermal Capacity (J/Kg · K)	Density (Kg/m^3)
Chip	Silicon	130	700	2329
Package	Plastic	0.2	900	2700
Solder Ball	60Sn-40Pb	50	150	9000
PCB	FR4	0.3	1369	1900
Pin	Aluminum	238	900	2700
Plane / Line	Copper	400	385	8960

The power density of the chip inside the package is assumed to be a time-variable function, which is given by

$$g(t) = f(t-30) + f(t-60) + f(t-90) \quad (28)$$

where

$$f(t) = A\cdot\exp\left(-\frac{t^2}{2\sigma^2}\right) \quad (29)$$

is the Gaussian pulse. The magnitude A is 5×10^7 W/m^3 and σ is set to 7 s. In (28), the superposition of three Gaussian pulses with different time-delay values (30, 60, and 90 s) is employed as the time-variable heat source, and the unit of time t is s.

The ambient temperature is assumed to be 25 °C. The boundary conditions on the top plane of the package, and the top and bottom planes of the PCB are imitated to be a convection boundary with a convective coefficient $h = 10$ W/(m^{2}K).

The transient thermal analysis is performed with the proposed LBFEM. At the observation time of 90 s, the temperature distribution on the surface of whole structure is described in Fig. 2(a). For comparison, the result of the commercial solver COMSOL is provided in Fig. 2(b). It is clear that the thermal profiles shown in these two figures are almost the same.

To illustrate the transient thermal response, two observation points (P1, P2) are placed in the structure. The point P1 locates the center of silicon chip inside the package, and P2 locates

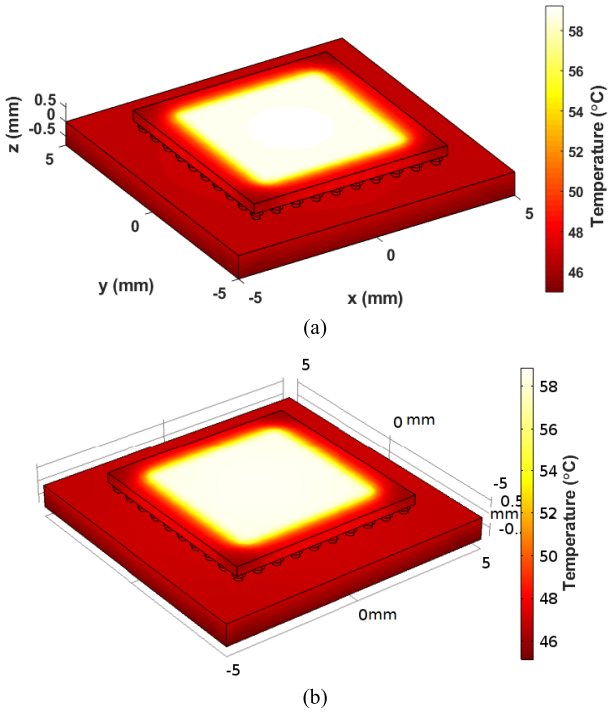

Fig. 2. Temperature distribution on the surface obtained by (a) LBFEM and (b) COMSOL.

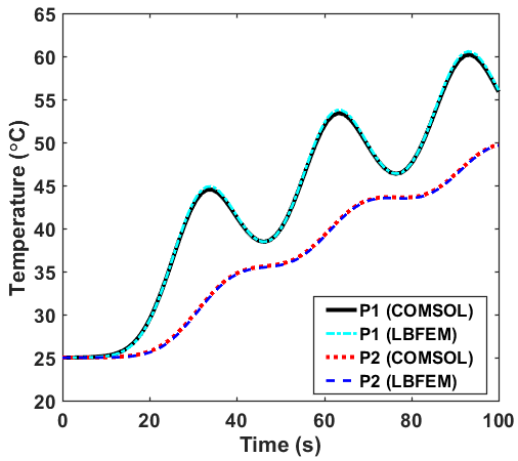

Fig. 3. Comparison of transient thermal responses at two observation points.

the dielectric layer of PCB. The specific coordinates of them are (0, 0, 0.475 mm) and (0, 0, −0.4 mm), respectively. The transient responses at the observation points are described in Fig. 3. The transient results obtained by the commercial solver COMSOL are also depicted for comparison. It is observed that the corresponding results are in good agreement. For efficiency, the CPU time of LBFEM is 126 s, while that of COMSOL is 963 s.

To further verify the capability and efficiency of the proposed algorithm, a more complex system with 3×3 FOWLP array is investigated, as shown in Fig. 4. The time-variable heat sources and boundary conditions are equal to those in the previous case. The simulated thermal profile at the observation time of 90 s is depicted and compared with that of

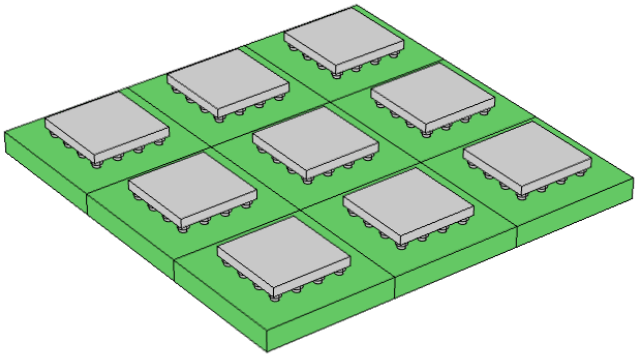

Fig. 4. Complex system with FOWLP array.

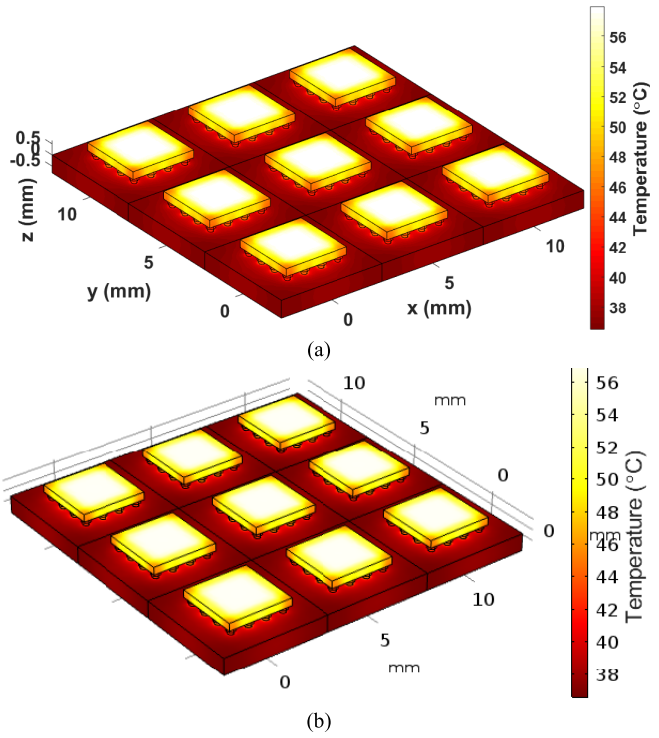

Fig. 5. Temperature distribution on the surface of FOWLP array obtained by (a) LBFEM and (b) COMSOL.

TABLE II
SIMULATION TIME OF LBFEM AND COMSOL

Number of Unknowns	LBFEM	COMSOL
354695	2 m 28 s	17 m 29 s
1066568	7 m 21 s	58 m 6 s
2845989	19 m 44 s	2 h 51 m 31 s

COMSOL in Fig. 5. Good agreement is observed. With respect to efficiency, the simulation times with different number of unknowns are listed in Table II. It is obvious that the LBFEM is much faster than COMSOL.

B. Surface-Mount Package on Circuit Board

The second example investigates the thermal situation for a silicon chip in a surface-mount package placed on a PCB close

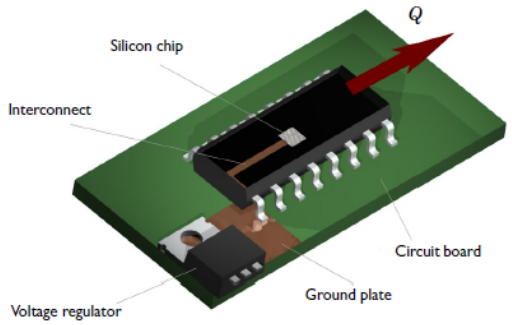

Fig. 6. Layout of the simulated silicon device, its package, and a voltage regulator [19].

to a hot voltage regulator [19]. The whole structure is shown in Fig. 6. The package connects to a PCB with 16 aluminum pins, and a silicon chip locates in the center of the package. Through an interconnect and one pin, the chip connects to a ground plane, where a heat generating voltage regulator is mounted. Thus, the voltage regulator may lead to overheating of system and affect the performance of silicon chip by the conducted heat.

The dimensions of PCB, plastic package, and silicon chip are $20\times20\times1$ mm^3, $9.9\times3.9\times1.5$ mm^3, and $1\times1\times0.1$ mm^3, respectively. The materials and corresponding thermal properties are listed in Table I. Note that the ground plane (with a thickness of 0.1 mm) of PCB, as well as the interconnect line (with a thickness of 0.02 mm) within the package, is treated by the thin-layer boundary condition due to its thin conducting layer.

Since the whole structure of this example is exposed to the air, the convection boundary is applied at the surface with $h = 10$ W/(m^2 K) and the ambient temperature of 30 °C. Note that the heat generating voltage regulator is treated by setting a fixed temperature (50 °C) at that surface of ground plane. The power density of the chip is assumed to be a time-variable function $g(t)$, as described in (28) and (29), where the magnitude A is 2×10^8 W/m^3, and σ is set to 7 s.

With the proposed method, the transient thermal simulation is implemented efficiently. At the observation time of 90 s, the temperature distribution of structure is described in Fig. 7(a). The result of COMSOL is provided for comparison, as shown in Fig. 7(b). Good agreement is observed between them.

Since the silicon chip is connected with ground plane of PCB (mounted with voltage regulator) through the interconnect and pin, in order to investigate the impact of regulator on thermal performance of chip, we then remove the regulator from the system. The transient thermal responses at the observation point in the center of silicon chip are compared in Fig. 8. We observe that the impact of voltage regulator is obvious. The difference of peak temperatures of two cases is larger than 4 K. At the observation time of 90 s, the temperature profile of the structure is illustrated in Fig. 9. For clarity, we only provide the temperature distribution in the package. It is observed that the temperature of the chip decreases apparently without the heat generated by the voltage regulator.

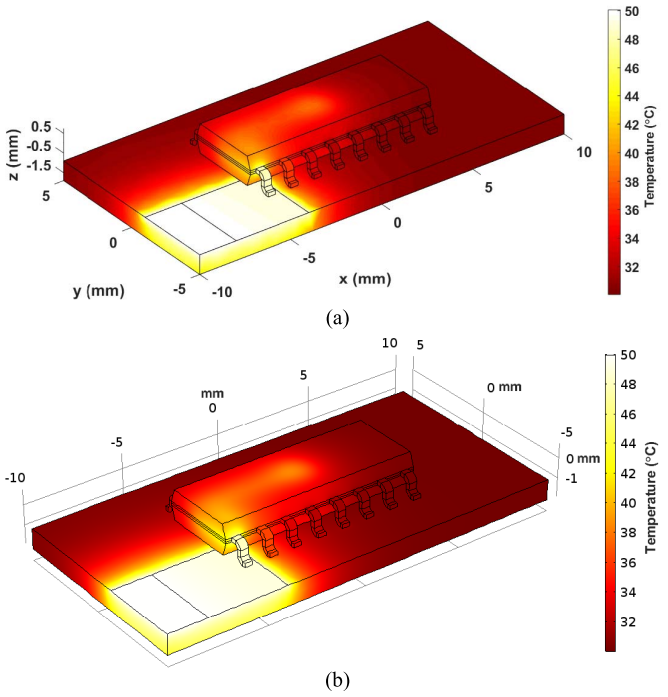

Fig. 7. Temperature distribution on the surface obtained by (a) proposed method and (b) COMSOL.

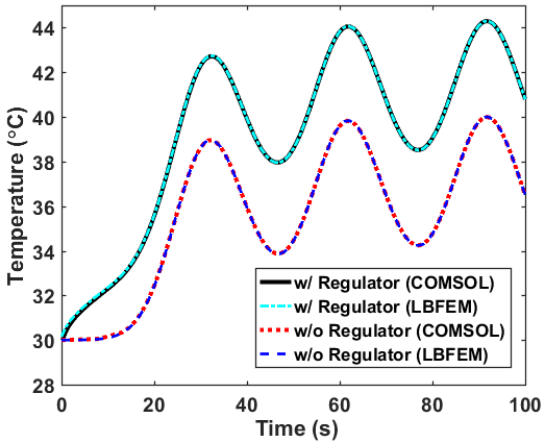

Fig. 8. Comparison of transient thermal responses in the center of chip.

C. Stacked 3-D ICs

The third example is associated with the thermal management of vertically stacked 3-D ICs [20]. A three-die stacked structure is described in Fig. 10. The dimensions of the whole structure are $10 \times 10 \times 2.9$ mm^3. The top layer is the thermal interface material (TIM) with a thickness of 0.5 mm, and below there are three die layers. The thickness of each one is 0.5 mm. Between the die layers is the underfill with a thickness of 0.3 mm. The above stacked 3-D ICs actually comprise a four-core accelerated processing unit which integrates graphic processing and core computing capabilities. The thermal properties of materials are listed in Table III.

In thermal simulation, the convection boundary is applied at the surface of structure with $h = 10$ W/(m^2 K) and the ambient temperature is 25 °C. A heat sink is attached on the

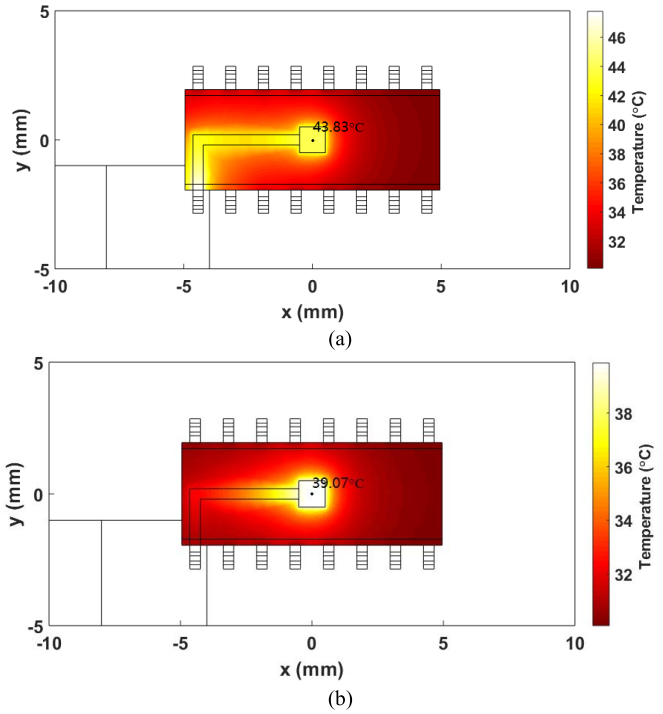

Fig. 9. Thermal distribution in the package (a) with impact of regulator and (b) without impact of regulator.

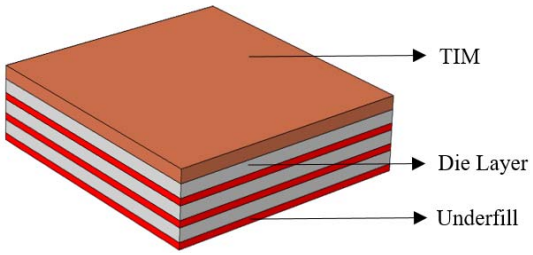

Fig. 10. Schematic of the stacked 3-D IC.

TABLE III
PROPERTIES OF MATERIALS IN STACKED 3-D ICS

Component	Thermal Conductivity (W/m · K)	Thermal Capacity (J/Kg · K)	Density (Kg/m^3)
Die	110	700	2329
Underfill	2.5	490	3765
TIM	1.6	610	3100

top of the dies with TIM. Therefore, the Dirichlet boundary with constant temperature of 25 °C is imposed on it.

For thermal management of the stacked ICs, two possible layouts are considered, as shown in Fig. 11 [20]. The first one places the cores in dies 2 and 3, and the graphics processing unit (GPU) in die 1. The second one moves the cores to die 1 and places the GPU in die 2. Various blocks and the power densities are also illustrated in the figure. The power density is assumed to be a time-variable function described in (28), and (29). For the cores with g_1 (t), the magnitude A is

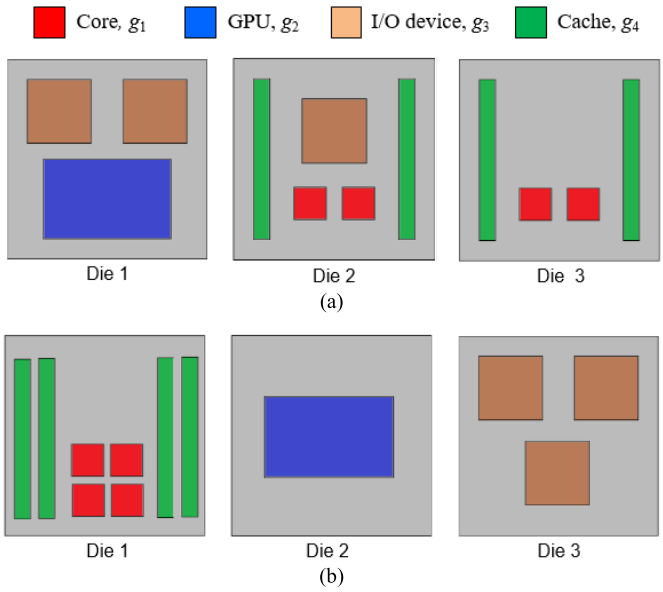

Fig. 11. Power distribution in each die layer. (a) Layout 1. (b) Layout 2 [20].

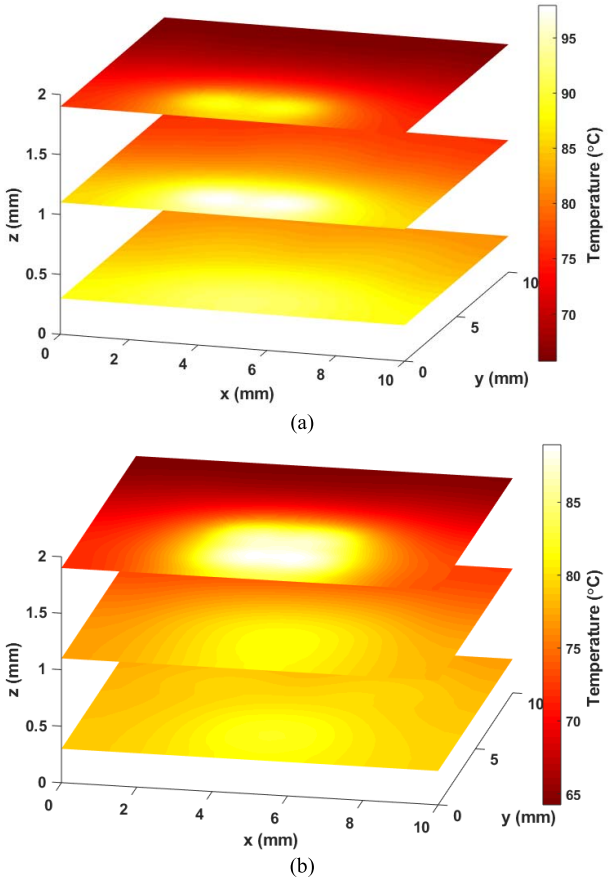

Fig. 12. Thermal map of each die layer for (a) layout 1 and (b) layout 2.

1.8×10^9 W/m^3. For the GPU with g_2 (t), A is 1×10^8 W/m^3. In g_3 (t) and g_4 (t), the magnitudes are 1.5×10^8 W/m^3 and 1.2×10^8 W/m^3, respectively.

The 2-D temperature distributions of die layers are described in Fig. 12. For the first layout case, the proximity

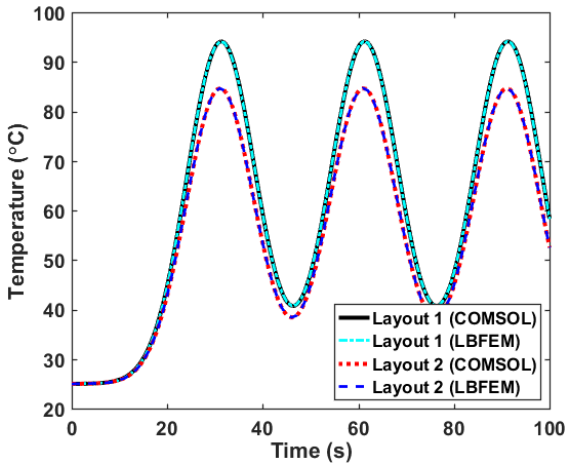

Fig. 13. Comparison of maximum temperatures in the structure as a function of time.

of cores in dies 2 and 3 results in a large local power density, and thus apparent temperature rise in the structure is observed. For comparison, by moving the cores close to the heat sink with the second layout strategy, the hotspot temperature of the second case is reduced by about 10 °C. Of course, it is a better choice for thermal management.

To illustrate the transient thermal responses of these two layouts, the maximum temperatures with the variation of time are depicted in Fig. 13. It is observed that the results of the proposed method are in very good agreement with the results of COMSOL. The maximum relative error is less than 0.5%. By comparison, the proposed LBFEM holds an obvious advantage with respect to the computational efficiency. In transient thermal simulation, the CPU time of LBFEM is 41 s, while that of COMSOL is 282 s.

V. Conclusion

An efficient algorithm based on LBFEM is developed in this article for transient thermal simulation of ICs and packages. With the weighted Laguerre polynomials and Galerkin testing procedure, a marching-on-in-order scheme in the Laguerre domain is derived, which is unconditionally stable. Combining with the FEM, the Laguerre coefficients are determined, and transient thermal responses of complex structures are readily obtained. The typical thermal boundary conditions, as well as the thin-layer case, are also derived in the Laguerre domain. Numerical results show that the proposed method is accurate and efficient for transient thermal simulation of complicated ICs and packages.

References

[1] Y. Zhang, Y. Zhang, and M. S. Bakir, "Thermal design and constraints for heterogeneous integrated chip stacks and isolation technology using air gap and thermal bridge," *IEEE Trans. Compon., Packag., Manuf. Technol.*, vol. 4, no. 12, pp. 1914–1924, Dec. 2014.

[2] Y.-B. Shi, W.-Y. Yin, J.-F. Mao, P. Liu, and Q. H. Liu, "Transient electrothermal analysis of multilevel interconnects in the presence of ESD pulses using the nonlinear time-domain finite-element method," *IEEE Trans. Electromagn. Compat.*, vol. 51, no. 3, pp. 774–783, Aug. 2009.

[3] T. Lu and J.-M. Jin, "Thermal-aware high-frequency characterization of large-scale through-silicon-via structures," *IEEE Trans. Compon., Packag., Manuf. Technol.*, vol. 4, no. 6, pp. 1015–1025, Jun. 2014.

[4] T. Lu and J.-M. Jin, "Transient electrical-thermal analysis of 3-D power distribution network with FETI-enabled parallel computing," *IEEE Trans. Compon., Packag., Manuf. Technol.*, vol. 4, no. 10, pp. 1684–1695, Oct. 2014.

[5] N. Li, J. Mao, W.-S. Zhao, M. Tang, W. Chen, and W.-Y. Yin, "Electrothermal cosimulation of 3-D carbon-based heterogeneous interconnects," *IEEE Trans. Compon., Packag., Manuf. Technol.*, vol. 6, no. 4, pp. 518–526, Apr. 2016.

[6] J. Xie and M. Swaminathan, "Electrical-thermal co-simulation of 3D integrated systems with micro-fluidic cooling and joule heating effects," *IEEE Trans. Compon., Packag., Manuf. Technol.*, vol. 1, no. 2, pp. 234–246, Feb. 2011.

[7] A. Cebula and D. Taler, "Finite volume method in heat conduction," in *Proc. Encyclopedia Therm. Stresses*. Amsterdam, The Netherlands: Springer, 2014, pp. 1645–1658.

[8] Z. Liu, S. Swarup, S. X.-D. Tan, H.-B. Chen, and H. Wang, "Compact lateral thermal resistance model of TSVs for fast finite-difference based thermal analysis of 3-D stacked ICs," *IEEE Trans. Comput.-Aided Design Integr. Circuits Syst.*, vol. 33, no. 10, pp. 1490–1502, Oct. 2014.

[9] R. Zhang, M. R. Stan, and K. Skadron, "HotSpot 6.0: Validation, acceleration and extension," Univ. Virginia, Charlottesville, VA, USA, Tech. Rep. CS-2015-04, 2015.

[10] M. N. Ozisik, *Finite Difference Methods in Heat Transfer*. New York, NY, USA: CRC Press, 1994.

[11] Y. Shao, Z. Peng, and J.-F. Lee, "Thermal-aware DC IR-drop co-analysis using non-conformal domain decomposition methods," *Proc. Roy. Soc. A*, vol. 468, no. 2142, pp. 1652–1675, Jun. 2012.

[12] Y. Shao, Z. Peng, and J.-F. Lee, "Thermal analysis of high-power integrated circuits and packages using nonconformal domain decomposition method," *IEEE Trans. Compon., Packag., Manuf. Technol.*, vol. 3, no. 8, pp. 1321–1331, Aug. 2013.

[13] J. Xie and M. Swaminathan, "System-level thermal modeling using nonconformal domain decomposition and model-order reduction," *IEEE Trans. Compon., Packag., Manuf. Technol.*, vol. 4, no. 1, pp. 66–76, Jan. 2014.

[14] Y. Saad, *Iterative Methods for Sparse Linear Systems*. Bangkok, Thailand: SIAM, 2000.

[15] P. Li, Y. Dong, M. Tang, J. Mao, L. J. Jiang, and H. Bagci, "Transient thermal analysis of 3-D integrated circuits packages by the DGTD method," *IEEE Trans. Compon., Packag., Manuf. Technol.*, vol. 7, no. 6, pp. 862–871, Jun. 2017.

[16] T.-Y. Wang and C. C.-P. Chen, "3-D thermal-ADI: A linear-time chip level transient thermal simulator," *IEEE Trans. Comput.-Aided Design Integr. Circuits Syst.*, vol. 21, no. 12, pp. 1434–1445, Dec. 2002.

[17] S. Liu, C. Wang, Z. Yu, W. Tang, and W. Zhuang, "Thermal-WLP: A transient thermal simulation method based on weighted Laguerre polynomials for 3-D ICs," *IEEE Trans. Compon., Packag., Manuf. Technol.*, vol. 7, no. 3, pp. 405–411, Mar. 2017.

[18] M. Ha, K. Srinivasan, and M. Swaminathan, "Transient chip-package cosimulation of multiscale structures using the Laguerre–FDTD scheme," *IEEE Trans. Adv. Packag.*, vol. 32, no. 4, pp. 816–830, Nov. 2009.

[19] *COMSOL Multiphysics User's Guide*, COMSOL Multiphysics 5.3a, Burlington, MA, USA, Dec. 2017.

[20] L. Choobineh and A. Jain, "Analytical solution for steady-state and transient temperature fields in vertically stacked 3-D integrated circuits," *IEEE Trans. Compon., Packag., Manuf. Technol.*, vol. 2, no. 12, pp. 2031–2039, Dec. 2012.

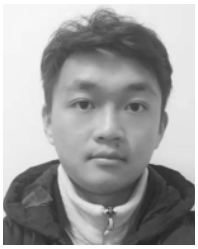

Bo Li received the B.S. degree in electronic science and technology from Shanghai Jiao Tong University, Shanghai, China, in 2018, where he is currently pursuing the M.S. degree in electromagnetic fields and microwave techniques.

His current research interests include computational electromagnetics and multiphysics modeling of integrated systems.

Min Tang (Member, IEEE) was born in 1980. He received the B.S. degree in electronic engineering from Northwestern Polytechnical University, Xi'an, China, in 2001, the M.S. degree in electrical engineering from Xi'an Jiao Tong University, Xi'an, in 2004, and the Ph.D. degree in electronic engineering from Shanghai Jiao Tong University, Shanghai, China, in 2007.

Since 2007, he has been a Faculty Member with Shanghai Jiao Tong University, where he is currently an Associate Professor with the Department of Electronic Engineering. He was a Post-Doctoral Research Fellow with the University of Hong Kong, Hong Kong, from 2010 to 2012. His research interests include signal and power integrity of high-speed circuits, multiscale and multiphysics modeling of integrated systems.

Haikun Yue received the B.S. degree in communication engineering from Xidian University, Xi'an, China, in 2010, and the Ph.D. degree in electromagnetic fields and microwave technology from the Huazhong University of Science and Technology, Wuhan, China, in 2016.

He joined the Microsystem and Terahertz Research Center (MTRC), China Academy of Engineering Physics (CAEP), Chengdu, China, in 2016. His current research focuses on terahertz microsystem.

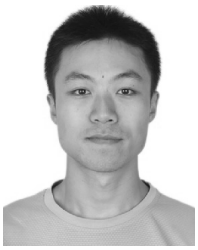

Yang Tang received the B.E. degree in micro and nano electronics from Tsinghua University, Beijing, China, in 2007, and the Ph.D. degree from the Institute of Microelectronics, Tsinghua University, in 2014.

He is currently an Associate Researcher with the Microsystem and Terahertz Research Center (MTRC), China Academy of Engineering Physics (CAEP), Chengdu, China. His areas of research focus on modeling and design for millimeter-wave and terahertz system on chip (SoC) and system in package (SiP) applications.

Junfa Mao (Fellow, IEEE) was born in 1965. He received the B.S. degree in radiation physics from the National University of Defense Technology, Changsha, China, in 1985, the M.S. degree in experimental nuclear physics from the Shanghai Institute of Nuclear Research, Chinese Academy of Sciences, Beijing, China, in 1988, and the Ph.D. degree in electronic engineering from Shanghai Jiao Tong University, Shanghai, China, in 1992.

Since 1992, he has been a Faculty Member with Shanghai Jiao Tong University, where he is currently a Chair Professor and the Vice President. He was a Visiting Scholar with the Chinese University of Hong Kong, Hong Kong, from 1994 to 1995, and a Post-Doctoral Researcher with the University of California at Berkeley, Berkeley, CA, USA, from 1995 to 1996. He has authored or coauthored more than 500 articles (including more than 130 IEEE journal articles). His research interests include the interconnect and package problems of integrated circuits and systems, analysis and design of microwave components and circuits.